Journal of the Chinese Society of Mechanical Engineers, Vol.47, No.5, pp 459~471 (2026)

Design of the Deflector Disc Valve for Static Push Vertical Drilling Tool

Rui Zhang *, Feng Sun **, Yifeng Wang ***, Ruiwen Feng **** and Yifan Yang ****

Keywords: Static push vertical drill tool; Annular disc valve; Finite element; Horizontal bench test

ABSTRACT

Under the technical background of static push vertical drilling tool, the design targeted at its key component - the annular disc valve is carried out. According to the friction force calculation of the disc valve, it is considered to design the valve seat structure in the form of a convex platform. Based on the finite element analysis, the clearance between the upper and lower plate valves and the height of the valve seat convex platform are determined. The annular valve structure and its flow path are further designed based on the quick shutdown response of the high and low sides of the hole. The horizontal bench test is carried out to verify its reliability. The results show that: In order to reduce the friction area of the disc valve, the two-layer combination designing is considered. The upper special-shaped hole with convex platform, and the lower special-shaped side channel structure are designed. The cemented carbide material is used to mould. The clearance between the upper and the lower disc valve should be controlled at 0.5mm, and the height of the disc valve convex platform should be controlled at 0.25mm accordingly. The horizontal bench test verifies the sealing and diversion effect of the valve. This paper provides reference for the design of vertical drilling tools.

Paper Received September, 2024. Revised July, 2025. Accepted September, 2025. *Corresponding author: Rui Zhang, Email: zhangrui@upc.edu.cn*

* *Professor, College of Petroleum Engineering, China University of Petroleum (East China), Qingdao, 266580, China*
State Key Laboratory of Deep Oil and Gas, China University of Petroleum (East China), Qingdao 266580, China

** *Senior Engineer, SINOPEC Research Institute of Petroleum Engineering Co., LTD, Beijing 102206, China*
National Key Laboratory of Shale Oil and Gas Enrichment Mechanism and Efficient Development, Beijing 102206, China

*** *Engineer, Geosteering & Logging Research Institute, Sinopec Matrix Corporation, Qingdao, 266071, China*

**** *Graduate Student, College of Petroleum Engineering, China University of Petroleum (East China), Qingdao, 266580, China*
State Key Laboratory of Deep Oil and Gas, China University of Petroleum (East China), Qingdao 266580, China

INTRODUCTION

With the deepening contradiction between energy supply and demand in the world, anti-inclined and drilling efficiency maintaining of high steep structure, anti-collision and straightening of unconventional infill well factory and offshore high density cluster well, and anti-slant and rapid development in high temperature and high pressure environment under the urgent need of safe and efficient development of dry hot rock geothermal resources, can greatly influence the application requirements of drilling straight wells, which makes the conventional deviation control technology not applicable than before(Biscaro et al., 2015; Zhang, 2003). There is an urgent need for a low-cost mechanical vertical drilling tool suitable for high speed, high reliability and high temperature conditions (Bai & Su, 1990; Liu et al., 2008).

In 1954, the German KTB drilling project developed the Automatic Vertical Drilling System (VDS), which effectively solved the problem of well deviation in high and steep structures. Subsequently, systems such as the Verti-Trak system from Baker Hughes, the PowerV series from Schlumberger, and the Geo-Pilot system from Halliburton were successfully applied to vertical drilling in highly inclined formations (Liu et al., 2008; Wang et al., 2024; Zhou & Yao, 2003). Currently, automatic vertical drilling tools can be classified into three types: static push-off bit type, dynamic push-off bit type, and target bit type. In China, Academician Su Yibian proposed the concept of downhole control engineering earlier, and together with Li Songlin et al., they proposed an integrated mechanical-electrical-hydraulic automatic vertical drilling design scheme. In 2003, in collaboration with Wuhan University of Science and Technology, they developed the AADDS-I type vertical drilling tool (Li & Su, 1999; Su, 2005). The

VDT5000 automatic vertical drilling system developed by the Bohai Drilling Company of China National Petroleum Corporation successfully underwent trial application in the Keshen 207 well in Tarim. The fiber-optic automatic vertical drilling system (AVDS) of the Drilling Technology Research Institute of Shengli Oilfield of Sinopec, which adopts a dynamic push-off method, as well as a new fusion algorithm and high-performance sensor components, has achieved excellent application results in the Anshun 1 well (Yang et al., 2020; Peng et al., 2006; Peng et al., 2024). However, these tools all employ relatively complex control systems and electronic components, which limit the control accuracy and lifespan of the tools, have high development costs, and are difficult to promote.

The table 1 below presents a comparison of the performance parameters of various existing drill-down systems.

Table 1 Comparison of Performance Parameters of Automatic Vertical Drilling System

AVDS	Sinopec AVDS	SLB PowerV	Bakerhuges Verti-Trak	CNPC BH-VDT
Wellbore	$12^1/4$" $8^1/2$"	$5^1/2$"--28"	$8^1/2$"--28"	$8^1/2$"--$21^1/2$"
Release the drilling pressure	yes	yes	yes	yes
Push-back mode	Modulation of dynamics	Modulation of dynamics	Static pushback	Static pushback
Power source	Plasticity pressure drop	Plasticity pressure drop	Electro-hydraulic control	Electro-hydraulic control
Working temperature	≤100℃	≤150℃	≤150℃	≤125℃
Stationary or slowly moving outer cylinder	no	no	yes	yes
Speed requirement	200r/min	220r/min	250r/min	250r/min
The position of the trailing edge ribs	Rotating outer cylinder	Rotating outer cylinder	Stationary or slowly moving outer cylinder	Stationary or slowly moving outer cylinder
Wing rib structure	Hinged type	Hinged type	Straight-up umbrella shape	Straight-up umbrella shape
Screw	no	Specialized screw	Specialized screw	screw
The downtime-free operating time in the underground environment	≥100h	≥200h	≥200h	≥150h

The static push (The tool generates continuous lateral thrust through its mechanical structure, enabling automatic deviation correction control of the wellbore trajectory without requiring additional power input during the drilling process) mechanical automatic vertical drilling tool achieves active real-time closed-loop deviation prevention and correction in the well by means of the interaction between the weight block and the annular disc valve(A disc-shaped valve involving the control of fluid flow and the regulation of pushing force) through a mechanical automatic downhole drilling tool (Jia et al., 2023; Shi et al;, 2021; Bi et al., 2022; Di et al., 2021). It retains the technical characteristics of low cost and high temperature - pressure resistance of the pure mechanical structure, while also possessing technical advantages such as resistance to strong vibration and dynamic control accuracy. The application effect in the field is good (Bi et al., 2021; Wang et al., 2021; Zhu et al., 2019). The annular disc valve, as one of the important core components of the static push-downhole drilling tool, its friction design determines the flow diversion and guiding effect, the gap between the discs determines the sealing effect, and it is the core control section where the weight mechanism acts on the push mechanism. The design quality of this

component is one of the key factors affecting the overall reliability of the static push-downhole drilling tool. Based on the static push technology, this paper conducts analysis and finite element analysis of the friction resistance of the annular disc valve and the annular valve gap, and improves the calculation and optimization design of the shut-off law. The structure and flow path design of the annular disc valve have been completed.

OVERALL STRUCTURE AND WORKING PRINCIPLE OF STATIC PUSHING TOOL

The mechanical static push automatic vertical drilling tool is a purely mechanical structure (Shi et al., 2019; Ramalakshmi & Dodagoudar, 2018; Shi et al., 2018; Li et al., 2018), which consists of gravity bias stabilization platform, double interlocked push-up wing rib, power mandrel, PDC composite bearing and other components. It is a three-layer independent rotating system that can actively prevent and correct inclination in the drilling process and is a closed-loop drilling tool (Shi et al., 2017; Li et al., 2015; Olav, 2015; Hyland et al., 2018). Its specific composition is shown in Figure 1:

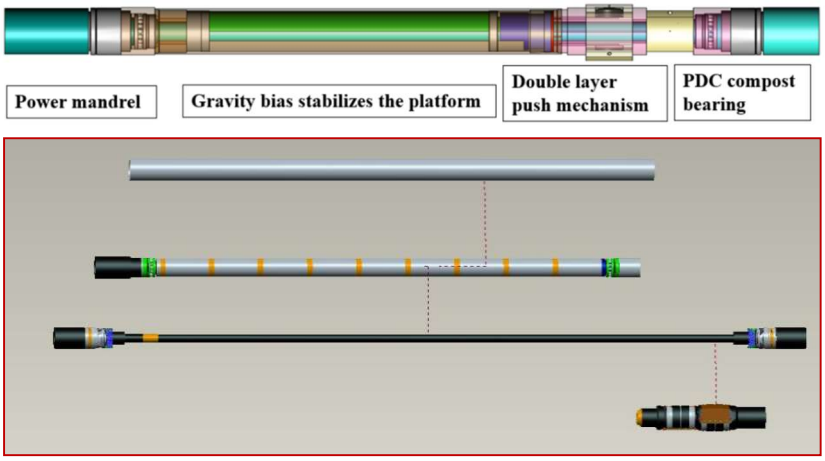

Fig.1 Schematic diagram of static pushing tools

The tool dynamically responds to deviation changes with a gravity bias platform with a response accuracy of 1º. The power mandrel transmits the bit weight torque and isolates the vibration and shock caused by the bit breaking rock. Filtered high pressure drilling fluid with small displacement can purify the bearing and provide power source for the push mechanism; The double-layer static pushing mechanism installed near the bit makes use of the water pressure difference of the bit to push against the well wall quasi-static, and the pushing force can reach more than 1t. Its working principle is shown in Figure 2:

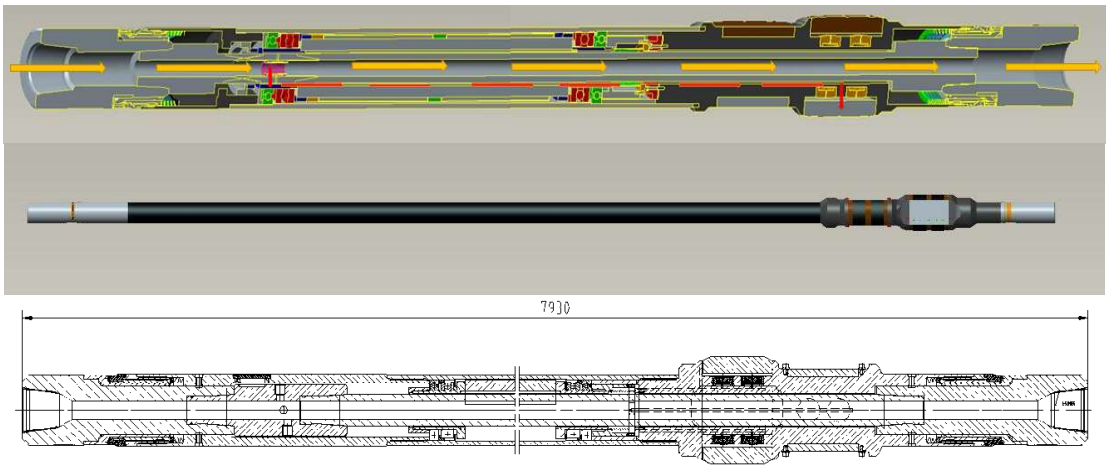

Fig.2 Description of the working principle of the static push tool

Static push mechanical vertical drilling tool is mainly used to solve the problem of anti-slant and straightening of straight well section in oil and gas well engineering. In actual drilling, the lower end of the tool is directly connected to the drill bit, and the upper end is connected to the conventional drill tool and screw. Through the mandrel, the adjustment of drilling engineering parameters such as high bit weight and high rotational speed is realized. The guide outer barrel set on the mandrel is not affected by it, and is basically in a static or slow rotating state, to achieve effective static push on the drill tool. When the well inclination exceeds the standard, the biased block located in the outer guide barrel rotates under the action of gravity, driving the upper annular valve at the lower end to the lower side direction of the tool and keeping it within a certain range of dynamic stability accuracy. The flow channel at the higher side direction of the lower annular valve is opened, and the small displacement drilling fluid flows into the high-pressure flow channel at the high side of the outer guide barrel and enters the corresponding piston cavity. Then it will Push the piston to slide along the radial direction, drive the wing rib to extend out, push against the wall statically, exert static pushing force on the high side of the hole, and push the drill tool to the direction of the low side of the hole, so as to realize the deviation correction during drilling.

DESIGN OF ANNULAR DISC VALVE STRUCTURE AND FLOW PATH

Calculation of the friction resistance between disc valves

(1) Calculation of friction force

The friction resistance moment between the disc valve is generated by the pressure difference between the upper and the lower disc valves and the relative rotation of valves. The traditional structure of the upper disc valve is shown in Figure 3.

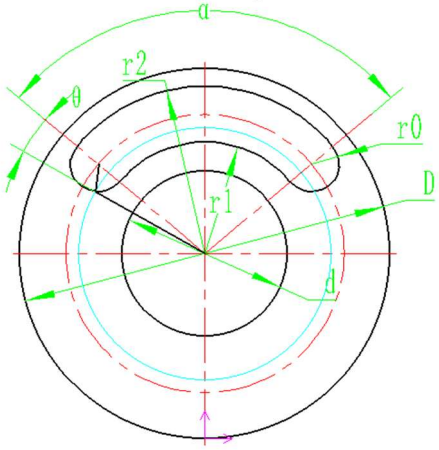

Fig.3 Structure diagram of upper disk valve

The friction resistance moment between the disc valve can be divided into three parts for calculation, namely:

$$T_p = T_{p1} + T_{p2} + T_{p3} \tag{1}$$

In this equation, T_{p1} — Frictional resisting moment when radius of upper disk valve meet: d/2 < r < r_1, N·m; T_{p2}—Frictional resisting moment when radius of upper disk valve meet:$r_1 < r < r_2$, N·m; T_{p3}—Frictional resisting moment when radius of upper disk valve meet:$r_2 < r <$ D/2, N·m; r_1,r_2—The inner and outer radius of the upper disc valve waist type hole, mm; d—The inner radius of upper disk valve; D—The outer radius of upper disk valve.

When $d/2 < r < r_1$, take the increment of δr, and, $\delta_r \to 0$, then the part of the ring area A can be considered as:

$$A = 2p_i r\delta \tag{2}$$

The static pressure F_p on the area of this part is

$$F_P = PA = 2Pp_i r\delta_r \tag{3}$$

The static friction force F_f generated by this part is:

$$F_f = F_P \mu \tag{4}$$

The resulting static friction torque M_f is:

$$M_f = F_f r \tag{5}$$

After solving:

$$M_f = 2P\mu p_i r^2 \tag{6}$$

So when r locate at (d/2, r_1):

$$\begin{aligned} T_{p1} &= \int_{\frac{d}{2}}^{r_1} 2\mu p_i r^2 dr \\ &= \frac{2}{3} P\mu p_i (r^3 - \frac{d^3}{8}) \end{aligned} \tag{7}$$

When $r_1 \leqslant r \leqslant r_2$, θ could be calculated by the law of cosine：

$$\theta = \arccos[\frac{r^2 + r_1 r_2}{r(r_1 + r_2)}] \tag{8}$$

When $r_1 \leqslant r \leqslant r_2$, take the increment of δr, and, $\delta_r \to 0$, the part of the ring area A is:

$$A = (2p_i - \alpha - 2\theta) r\delta_r \tag{9}$$

Plug A into equation (3), and we can see:

$$F_p = PA = P(2p_i - \alpha - 2\theta) r\delta \tag{10}$$

and：

$$T_{p2} = \int_{r_1}^{r_2} P(2p_i - \alpha - 2\theta) r^2 dr \tag{11}$$

When $r_2 < r <$ D/2, it is the same with that when d/2< r <r_1, so this part of the friction torque is:

$$T_{p3} = \frac{2}{3} P\mu p_i (\frac{D^3}{8} - r_2^3) \tag{12}$$

The total friction torque of the disc valve is:

$$\begin{aligned} T_p &= \frac{2}{3} P\mu p_i (r_1^3 - \frac{d^3}{8}) + \frac{2}{3} P\mu p_i (\frac{D^3}{8} - r_2^3) \\ &+ \int_{r_1}^{r_2} P\left\{2p_i - \alpha - 2\arccos[\frac{r^2 + r_1 r_2}{r(r_1 + r_2)}]\right\} r^2 dr \end{aligned} \tag{13}$$

In this equation, μ-Coefficient of friction between disc valves; α-The opening Angle of the upper disc

valve waist type hole, ° .

(2) Results analysis of the friction calculation

Through the calculation results of the above formula, it can be seen that the static friction torque is proportional to the static friction coefficient μ and the hydrostatic pressure P, and is proportional to the cubic power of the radius R^3. In the actual design process, the static pressure P is often a fixed value, and the friction coefficient μ is generally a small value, and the reduced interval is relatively small. Therefore, reducing the value of the radius R is the most effective way.

From another perspective, the friction resistance of the disc valve is proportional to the square of the radius, and the square of the radius is the area of the disc valve, so the contact area of the disc valve is considered to be reduced. Therefore, the structure of the valve seat matched with the disc valve is considered as shown in Figure 4. The valve seat is in the form of a convex, the diameter of the convex is D_o, and the diameter of the center is D_f, and the number is 3. The friction calculation formula at the boss is shown in equation (14):

$$F_n = nPp_iR^2 \tag{14}$$

Where, n-number of boss, the value here is 3; P-Bit pressure drop, Mpa; R- radius of boss, the value here is $D_0/2$

Friction force here is:

$$F_f = F_n\mu_v \tag{15}$$

The frictional resisting moment is:

$$T_p = F_f\frac{D_f}{2} \tag{16}$$

Where, μ_v- Coefficient of friction between disc valves ; D_f - Distance between the center of the boss and the center of the mandrel, mm.

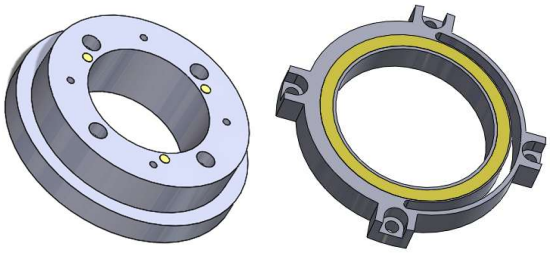

Fig. 4 Structure diagram of valve seat

In this design process, because the disc valve finally adopts the boss contact structure as shown in Figure 4, the working area of the upper and lower fluid pressure of the disc valve is greatly reduced, thus greatly reducing the role of the friction resistance between the disc valve. However, the existence of the convex inevitably leads to the gap between the upper and lower disc valves, resulting in certain discharge flow. The size of the discharge rate is directly related to the size of the lateral force (push force) on each push mechanism of the drill tool, and then has an impact on the deviation correction effect of the drill tool. Therefore, for the importance of the selection of the height of the convex, the gap flow between the upper and the lower disc valves generated by the height of the boss is simulated, and it is discussed in detail in the following chapters.

Finite element analysis of annular valve clearance

(1) Analytical methods and turbulence models

The influence of disc valve clearance on the flow field inside drill pipe is studied by computational fluid dynamics method (CFD). The pressure variation of the flow field in the drill under constant pump volume is simulated and analyzed. CFD discretizes with the finite volume method, derives the equation of motion which can be applied to the fluid in the flow field based on the three conservation laws of body motion. Assuming that the fluid is composed of infinitesimal, infinite, close to each other and continuous fluid particles of A continuous medium without A gap, if we take a random control body A (or fluid unit A), the law of conservation of mass, law of conservation of momentum, law of conservation of energy are shown in Figure 5, Figure 6 and Figure 7.

According to the law of conservation of mass, the mass flow out of the control body is equal to the mass reduction in the control body. If the mass reduction is defined as negative, the expression equation of mass conservation is as follows:

$$[\frac{\partial(\rho u)}{\partial x}+\frac{\partial(\rho v)}{\partial y}+\frac{\partial(\rho w)}{\partial z}]dxdydz = -\frac{\partial\rho}{\partial t}dxdydz \tag{17}$$

Where, u、v、w-he velocity of fluid flow in three directions x、y、z, m/s; ρ-Density of fluid, kg/m^3。

For incompressible fluids:

$$[\frac{\partial(u)}{\partial x}+\frac{\partial(v)}{\partial y}+\frac{\partial(w)}{\partial z}] = 0 \tag{18}$$

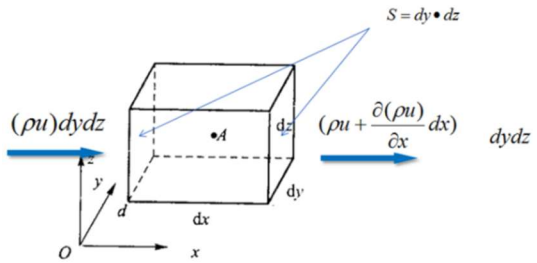

Fig. 5 Schematic diagram of mass conservation of control body

For the control body A, the force is composed of two parts: surface force and volume force. According to Newton's second law, the momentum conservation equation of the control body A in x, y and z directions can be obtained as follows:

$$\begin{cases} \rho\dfrac{Du}{Dt}=\dfrac{\partial p}{\partial x}+\dfrac{\partial \tau_{xx}}{\partial x}+\dfrac{\partial \tau_{yx}}{\partial y}+\dfrac{\partial \tau_{zx}}{\partial z}+\rho f_x \\ \rho\dfrac{Dv}{Dt}=\dfrac{\partial p}{\partial y}+\dfrac{\partial \tau_{xy}}{\partial x}+\dfrac{\partial \tau_{yy}}{\partial y}+\dfrac{\partial \tau_{zy}}{\partial z}+\rho f_y \\ \rho\dfrac{Dw}{Dt}=\dfrac{\partial p}{\partial z}+\dfrac{\partial \tau_{xz}}{\partial x}+\dfrac{\partial \tau_{yz}}{\partial y}+\dfrac{\partial \tau_{zz}}{\partial z}+\rho f_z \end{cases} \tag{19}$$

In the equation above, P-pressure, Pa; f_x、f_y、f_z-external force in x、y、z three directions, N; τ-tensor of stress.

Define tensor of stress as:

$$\overline{\overline{\tau}}=u_D[(\nabla\vec{v}+\nabla\vec{v}^{T})-\frac{2}{3}\nabla\vec{v}I] \tag{20}$$

Where, u_D-dynamic viscosity; I- unit tensor.

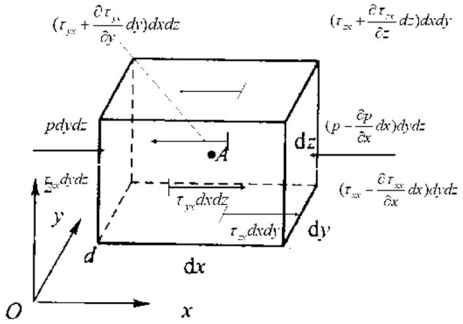

Fig.6 Schematic diagram of momentum conservation of the control body

According to the law of conservation of energy, the energy change rate in the control body A equals to the net heat flow into the control body plus the power of the volume force and surface force to do work on the control body, the energy conservation expression is as follows:

$$\begin{aligned} &\rho\frac{D}{Dt}(e+\frac{V^2}{2})=\rho q+\frac{\partial}{\partial x}(k\frac{\partial T}{\partial x})+\frac{\partial}{\partial y}(k\frac{\partial T}{\partial y}) \\ &+\frac{\partial}{\partial z}(k\frac{\partial T}{\partial z})-\frac{\partial(up)}{\partial x}-\frac{\partial(vp)}{\partial y}-\frac{\partial(wp)}{\partial z}+\frac{\partial(u\tau_{xx})}{\partial x} \\ &+\frac{\partial(u\tau_{yx})}{\partial y}+\frac{\partial(u\tau_{zx})}{\partial z}+\frac{\partial(v\tau_{xy})}{\partial x}+\frac{\partial(v\tau_{yy})}{\partial y}+\frac{\partial(u\tau_{zy})}{\partial z} \\ &+\frac{\partial(w\tau_{xz})}{\partial x}+\frac{\partial(w\tau_{yz})}{\partial y}+\frac{\partial(w\tau_{zz})}{\partial z}+\rho fV \end{aligned} \tag{21}$$

In this equation, e-total stockpile energy, J; T-temperature, ℃.

The mechanical governing equations of CFD can be obtained immediately and rewritten into the divergence form as

$$\begin{aligned} &\frac{\partial\rho}{\partial t}+\nabla(\rho\vec{V})=0 \\ &\rho\frac{d\vec{V}}{dt}=-\nabla p+\nabla\tau+\rho\vec{f} \\ &\rho\frac{de}{dt}=\nabla(\sigma\vec{V})+\nabla(k\nabla T)+\rho q \end{aligned} \tag{22}$$

Where, ▽- laplace operator.

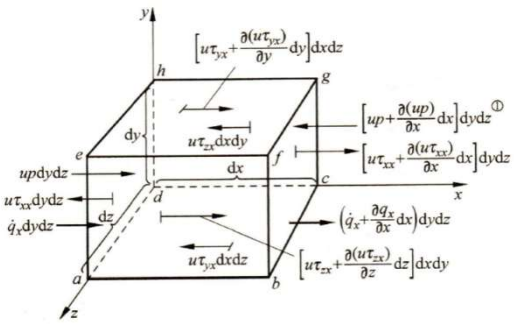

Fig. 7 Schematic diagram of control energy conservation

To solve the above equation, three supplementary equations need to be introduced, which are:

$$P=\rho RT \tag{23}$$

$$e=C_vT \tag{24}$$

$$e=e(T,P) \tag{25}$$

In the equations above, R-gas constant; C_v-specific heat capacity at constant volume.

The turbulence models applied in this paper is SST k-ω model. By using the k-ω model in the boundary layer and the k-ε model in the turbulent core region outside the boundary layer, this model can effectively predict the beginning point of fluid separation and the size of the separation region under the condition of inverse pressure gradient, and quickly obtain the convergence solution..

The turbulent kinetic energy transport equation and turbulent specific dissipation equation of SST k-ω model are as follows:

$$\frac{\partial\rho k}{\partial t}+\frac{\partial}{\partial x_j}[\rho u_j k-(\mu+\sigma_k u_t)]=\tau_{tij}S_{ij}-\beta^*\rho\omega k \tag{26}$$

$$\begin{aligned} &\frac{\partial\rho\omega}{\partial t}+\frac{\partial}{\partial x_j}[\rho u_j\omega-(\mu+\sigma_\omega u_t)\frac{\partial\omega}{\partial x_j}] \\ &=P_\omega-\beta_c\rho\omega^2+2(1-F_1)\frac{\rho\sigma_\omega}{\omega}\frac{\partial k\partial\omega}{\partial x_j\partial x_j} \end{aligned} \tag{27}$$

In the equations, k-Turbulent energy, J; $u_t=\dfrac{\rho k}{\omega}$ - eddy viscosity; τ_{tij}-reynolds stress, Pa; S_{ij}-mean velocity strain rate tensor; F_1, β_c, σ_k, σ_ω-model parameters; β^*-model constants; P_ω-Production phase：

$$P_\omega=2\gamma\rho(S_{ij}-\frac{\omega S_{nn}S_{ij}}{3})S_{ij} \tag{28}$$

In this equation, γ-model parameters

The eddy viscosity model of Reynolds stress is：

$$\tau_{tij}=2\mu_t(S_{ij}-\frac{S_{nn}S_{ij}}{3})-\frac{2}{3}\rho kS_{ij} \tag{29}$$

In this equation, S_{nn}-The Kronecker operator.

Taking water as an incompressible fluid medium (ρ=1.0kg/m^3), the Mach number is very low and the Reynolds number is very high. Based on the above analysis, the basic equations used for simulation analysis are as follows:

$$\rho(\vec{V}\nabla)\vec{V} = \nabla\{-p\vec{I} + [\mu+\mu_t][\nabla\vec{V} + (\nabla\vec{V})^T]\} + \vec{F}$$
$$\rho\nabla\vec{V} = 0$$
$$\rho(\vec{V}\nabla)k = [(\mu+\mu_t\sigma_k)\nabla k] + \rho - \beta^*\rho\omega k$$
$$\rho(\vec{V}\nabla)\omega = [(\mu+\mu_t\sigma_\omega)\nabla\omega] + \frac{\gamma}{\mu_t}\rho p - \rho\beta_c\omega^2 + 2(1-F_1)\frac{\sigma_{\omega 2}\rho}{\omega}\nabla k\nabla\omega \quad (30)$$

Where, $(\nabla\vec{V})^T$ -the corresponding function at temperature T.

Initialization equation of Wall distance is:

$$\nabla G\cdot\nabla G + \sigma_\omega G(\nabla\cdot\nabla G) = (1+2\sigma_\omega)G^4$$
$$l_w = \frac{1}{G} - \frac{l_{ref}}{2} \quad (31)$$

In the equations, G-Reciprocal wall distance, 1/m; l_{ref}-Reference proportional length.

The entry control equation is:

$$\vec{V} = -\frac{M_f}{\rho}\vec{n}$$
$$k = k_0, \omega = \omega_0, \nabla G\vec{n} \quad (32)$$
$$M_f = \frac{\rho V_L}{\pi R^2 t}$$

In the equations above, $\vec{n}$ -normal unit vector; M_f -point by point mass flow rate, kg/(m^2·s); V_L、R-the volume of fluid passing through the entrance per unit time and the radius of the entrance; t-time, s。

The export control equation is:

$$\vec{n}^T[-p\vec{I} + [\mu+\mu_T][\nabla\vec{V} + (\nabla\vec{V})^T]\vec{n} = -\bar{p}_0$$
$$\bar{p}_0 \le p_0, \vec{V}t = 0 \quad (33)$$
$$\nabla k\vec{n} = 0, \nabla\omega\vec{n} = 0$$

Where, $\bar{p}_0$ 、p_0—preset exit pressure and theoretical exit pressure, MPa。

In the simulation process, the fluid channel wall is set as no slip boundary condition, and the governing equation is as follows:

$$\vec{V} = 0; k = 0; \omega = \lim_{l_w\to 0}\frac{6\nu}{\beta_1\ell_w^2}, \ell_w = 0 \quad (34)$$

(2) Simulation analysis results

According to Bernoulli's equation:

$$P_L + \frac{1}{2}\rho_L v_L^2 + \rho_L gH = C \quad (35)$$

In this equation, P_L-internal fluid pressure in the flow field, MPa; ρ_L-density of drilling fluid, kg/m^3; v_L-drilling fluid flow rate, m/s; H-the distance of the flow position from the ground, m。

In the drilling process with constant pumping capacity, when the cross-sectional area of the flow field inside the drill tool changes, the drilling fluid pressure inside the drill tool before and after the cross-sectional area change due to the change of drilling fluid flow velocity (ignoring the change of the distance between the fluid flow position and the ground and the influence of the pressure drop inside the drill tool) changes ΔP_L:

$$\Delta P_L = P_{L1} - P_{L2} = \frac{1}{2}\rho_L\left(\frac{Q_L}{S_{D2}}\right)^2 - \frac{1}{2}\rho_L\left(\frac{Q_L}{S_{D1}}\right)^2 \quad (36)$$

Where, P_{L1}, P_{L2}-the pressure of the flow field before and after the change of the cross-sectional area of the flow field inside the drill, MPa; Q_L-drilling fluid flow, m^3/s; S_{D1}, S_{D2}-the cross-sectional area before and after the change of the cross-sectional area of the flow field inside the drill, m^2。

The design and process parameters for simulating the flow field inside the drilling tool are shown in Table 2. During the simulation and analysis process, the internal pressure drop of the drilling tool is mainly considered, so the pressure of drilling fluid in the annulus outside the drilling tool is ignored, and the outlet pressure is set at 0MPa. If the outlet at the piston clearance is not considered, the pressure drop of the flow field inside the drill tool is about 2.92MPa when the disk-free valve clearance is obtained. After setting the piston clearance as the outlet, the maximum pressure of the disc valve calculated by simulation is 2.16MPa, which is less than the theoretical calculation result and basically consistent with the actual situation, as shown in Figure 8.

Table 2 Design and process parameters for simulation of flow field inside drill pipe

serial number	designing parameter	parameter values	serial number	designing parameter	parameter values
①	entry radius, mm	58	④	flowin, L/min	1800
②	spout radius, mm	5	⑤	piston clearance, mm	0.1
③	Nozzles number	5	⑥	outlet pressure, MPa	0

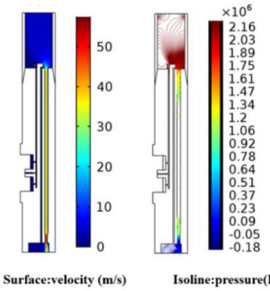

Fig.8 Velocity and pressure cloud image of flow field

when there is no gap between disc valves

When the gap of the disc valve is 0.2mm, 0.5mm, 1mm and 5mm, the flow rate and pressure cloud images of the flow field inside the drill tool are shown in Figure 9 respectively. It can be seen that with the gradual increase of disc valve clearance, the maximum flow rate and maximum pressure in the flow field inside the drill tool show a gradually decreasing trend, but the maximum flow rate and maximum pressure inside the drill tool basically maintain the same position, the maximum flow rate appears in the equivalent bit nozzle position, and the maximum pressure is located above the disc valve. Fig.10 is a partial enlarged diagram of the influence of disc valve clearance on the flow field near the disc valve. When the disc valve clearance is less than 0.5mm, the internal pressure of the low-pressure drilling fluid flow path is small, and the internal pressure of the low-pressure drilling fluid flow path gradually increases with the increase of disc valve clearance. The increase rate was significantly faster than that of < 0.5mm. When the disc valve gap is 5mm, the drilling fluid flow channel pressure on the right side of the disc valve is basically consistent, indicating that there is no low-pressure drilling fluid flow channel at this time, and the disc valve loses its sealing effect.

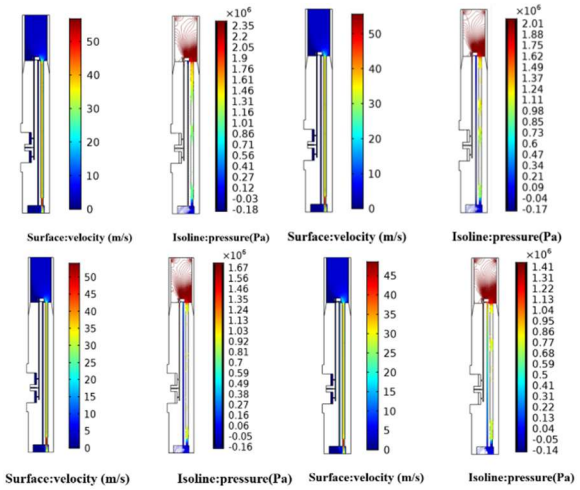

Fig.9 Velocity and pressure cloud image of the flow field inside the tool when the gap between the disc valves is 0.2 - 0.5 - 1 - 5mm

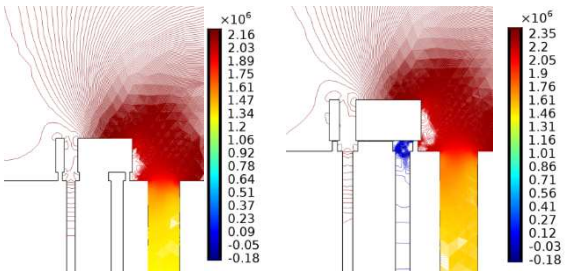

(a) 0 mm (b) 0.2 mm

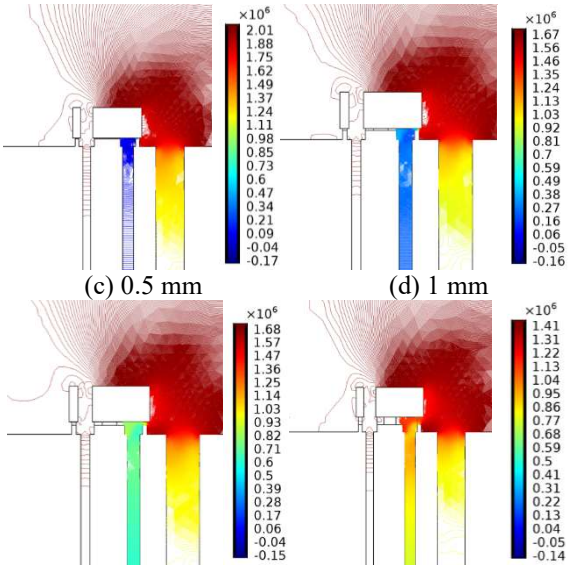

(c) 0.5 mm (d) 1 mm

(e) 2 mm (f) 5 mm

Fig.10 Local magnification of disc valve flow field with different gaps

As shown in Figure 11, the pressure difference on both sides of the drilling tool piston and the change trend of the drilling fluid channel pressure difference between the upper and lower sides of the hole under the disc valve vary with the gap between the disc valve. In order to ensure the normal operation of the drilling tool, the discharge rate of the disc valve must be strictly controlled, and the gap between the disc valve should be controlled below 0.5mm. At this time, the pressure in the drilling fluid channel on the lower side of the hole under the disc valve has little change when there is no gap between the drilling fluid channel and the disc valve. Under the premise of allowing a certain discharge rate of the disc valve, it can still play a certain "sealing" role and ensure the normal operation of the drilling tool. Finally, it is determined that the clearance of the upper and the lower disc valve should be controlled at 0.5mm, and the height of the disc valve boss should be controlled at 0.25mm respectively.

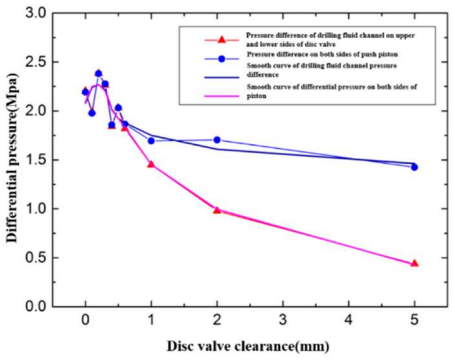

Fig.11 Pressure difference on both sides of piston and pressure difference of drilling fluid channel under disc valve under the influence of disc valve clearance

The structure and flow path design optimization of annular disc valve based on the quick shutdown response law of high and low sides of borehole

(1) Structure design optimization of annular disc valve

The annular disc valve mainly considers the passage space of the mandrel and the sliding area of the seal to minimize the sliding fit, so the design is a two-layer combination design. The upper part of the high-and-low-pressure flow channel is designed as a shaped hole, mainly considering the fast closing performance and reducing the sliding friction, the design is a shaped hole plus boss. According to the numerical calculation and simulation structure, design the shape of the high-and-low-pressure holes and specific structural dimensions such as the height and width of the boss, and finally achieve the design purpose of fast closing and low friction, as shown in Figure 12. In order to leave a large diameter mandrel space, the lower part of the valve is designed as a special-shaped side channel structure, and the position of the high-and-low-pressure channel holes is dislocated by 45° from the long hole position of the lower push mechanism, making full use of the redundant position of the push mechanism to ensure the structural size and safety check of the mandrel. The upper and lower parts of the lower annular disc valve in order to prevent fluid erosion damage, consider the use of cemented carbide material as a whole forming.

Fig.12 Double-layer split design of the upper and the lower disc valves structure

(2) Numerical calculation and analysis of the turn-off rule of annular disc valve

For tools with Φ178mm, the surface of the components on the lower disc valve adopts a 4mm waist hole, the convex side is 3mm, and the equivalent area is 80.68mm, which is slightly larger than the 10mm circular hole area of 78.5mm, and the offset is 7mm, the effect is equivalent to that of the circular hole 10mm offset 13mm. Figure 13 is a schematic diagram for calculating the flow path area of the footer valve under simulated on-off conditions.

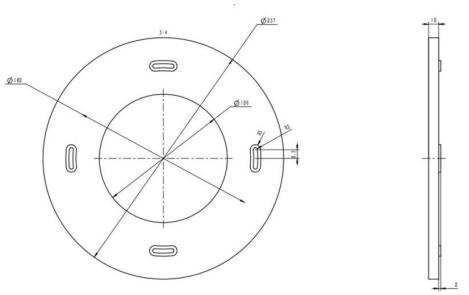

Fig.13 Schematic diagram for calculating the flow path area of the footer valve under simulated on-off conditions

In accordance with the linear pendulum motion mode, the on-going area of the upper disk valve is calculated according to the position change of 10° at an interval of 0-360°. The calculation results are shown in Table 3.

Table 3 Calculated values of conduction area at different angles

Angle/°	A/mm^2	B/mm^2	C/mm^2	D/mm^2
0	0	6.79	80.68	6.79
10	0	0	80.68	29.7
20	0	0	80.68	53.53
30	0	0	80.68	74.04
40	0	0	80.68	80.68
45	0	0	80.68	80.68
50	0	0	80.68	80.68
60	0	0	74.04	80.68
70	0	0	53.53	80.68
80	0	0	29.7	80.68
90	6.79	0	6.79	80.68
100	29.7	0	0	80.68
110	53.53	0	0	80.68
120	74.04	0	0	80.68
130	80.68	0	0	80.68
135	80.68	0	0	80.68
140	80.68	0	0	80.68
150	80.68	0	0	74.04
160	80.68	0	0	53.53
170	80.68	0	0	29.7
180	80.68	6.79	0	6.79
190	80.68	29.7	0	0
200	80.68	53.53	0	0
210	80.68	74.04	0	0
220	80.68	80.68	0	0
225	80.68	80.68	0	0
230	80.68	80.68	0	0
240	74.04	80.68	0	0
250	53.53	80.68	0	0
260	29.7	80.68	0	0
270	6.79	80.68	6.79	0
280	0	80.68	29.7	0
290	0	80.68	53.53	0
300	0	80.68	74.04	0
310	0	80.68	80.68	0
315	0	80.68	80.68	0
320	0	80.68	80.68	0
330	0	74.04	80.68	0
340	0	53.53	80.68	0
350	0	29.7	80.68	0
360	0	6.79	80.68	6.79

Further, Figure 14 shows the change of the turn-off area of the guide hole of the lower disc valve at different angles. It can be seen from the figure that when the upper disc valve is at the Angle of inclination of 0°, the diversion ports in the four directions are closed. When the azimuth is at an equal Angle of 90°/270° and the well inclination exceeds the control accuracy, the diversion port at this azimuth is in a fully open state, and the high-pressure fluid is pushed by the piston driving the wing rib at this azimuth. When the azimuth is between 0° and 90°, the diversion hole between 0° and 90° is partially opened, and the piston fins in both directions extend and push against the well wall at the same time to achieve effective pushing against the high side of the hole.

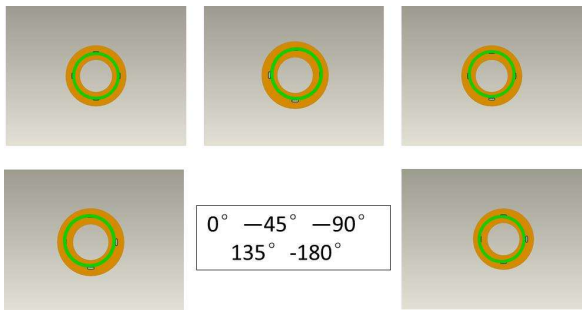

Fig.14 Change of surface price of backflow hole at different angles

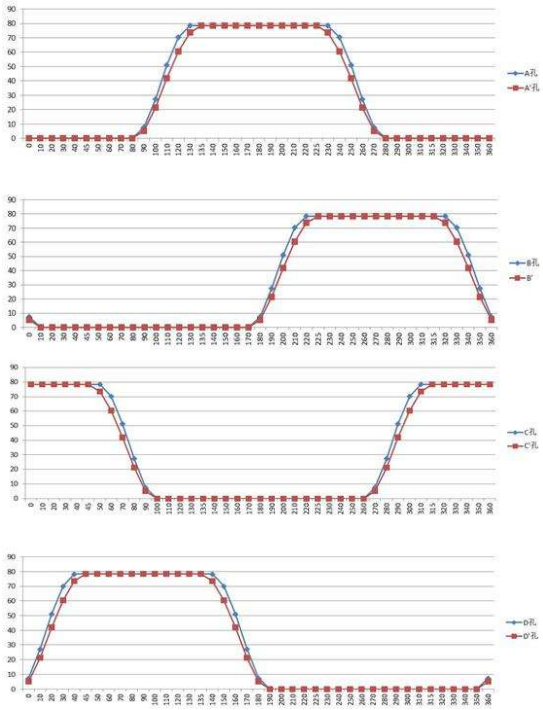

Fig.15 Closing curve of 4mm waist type 3mm convex hole compared to 4mm waist type 5mm convex hole

In the process of drilling, the upper disc valve, driven by the bias unit, moves with the surface of the lower disc valve in a linear pendulum motion. The quick closing of the diversion hole under different incline and different orientation plays an important role in the push and correction effect. The lower disc valve adopts the structural design of the convex waist hole, which can increase the conduction efficiency by 17% compared with the circular hole. Fig.15 shows the turn-off rule curve of the 4mm waist type 3mm boss hole changing with the orientation.

HORIZONTAL BENCH TEST

In order to verify the sealing condition of the upper and lower annular valve and the conduction condition of the high-pressure diversion hole at 90° inclination, and verify the conduction condition of the stable platform and the sealing condition of the annular valve under different rib pushing direction, the horizontal bench test is carried out.

Parameters of vertical drilling tools are as follows: 178 tool length: 6025mm; Max. weight: 1.8t, diameter: 178mm;

Test requirements: 90° inclination; pressure difference: 0-5Mpa; measurement parameters: pushing out starting pressure difference of push down wing rib, corresponding situations of push down wing rib under different directions, changes of pressure difference and pressure loss changes at TC of both ends under different displacement. As shown in Figure 16.

Fig.16 Horizontal bench test of 178mm vertical drilling tool

The relationship curve between pump pressure drop and nozzle pressure drop in tool test is shown in Figure 17:

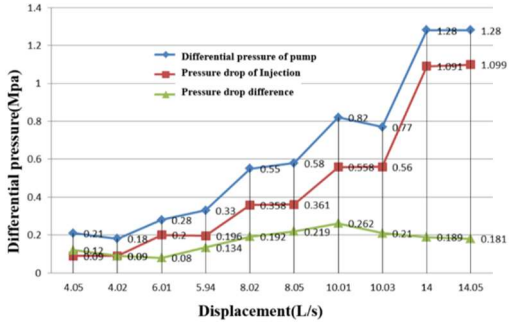

Fig.17 Relationship curves of different displacement with pump pressure drop and nozzle pressure drop

As we can see, the nozzle pressure drop increases

with the increase of displacement, which is the main factor of pump pressure drop. The pressure drop of the difference between the two tends to increase, but its increase is much smaller than the nozzle added value. Remove the pressure drop discharge value under the same conditions, and the relationship between pressure drop and displacement is shown in Figure 18:

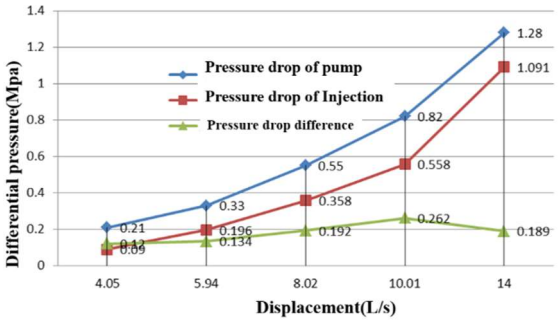

Fig. 18 Relationship curves of different displacement with pump pressure drop and nozzle pressure drop (data points with the same displacement are removed)

As we can see, during the test of tool 178, the pumping pressure gradually increased with the displacement. During the increase from 4.05L/s to 14L/s, the overall pumping pressure drop increased from 0.21Mpa to 1.28Mpa. The nozzle has a diameter of 20mm, and the calculated pressure drop is increased from 0.12Mpa to 1.091Mpa; The difference between the two is other pressure losses of the tool, which also increases slightly with the increase of displacement, from 0.09Mpa to 0.262Mpa, and at 14L/s displacement, it is 0.189, which is slightly reduced, and further verification is needed. The pressure difference shows that in addition to the nozzle pressure drop, a small part of the fluid leakage at the PDC thrust bearings at both ends of the tool also causes some pressure loss. The specific amount needs to calculate the specific pressure loss by calculating the pushing force of the wing rib.

Test results and analysis: the starting pressure of the wing rib of 178 tool is 0.3Mpa, which is about 847.8N.m. By adjusting the orientation of the push wing rib, the water outlet hole of the wing fin is observed. Only one push wing rib comes out of the water at the 90° orientation, indicating that the upper and lower annular valves of the stable platform are normally sealed, and only the high side diversion holes are open, and other holes are not open. When the outer cylinder is rotated to 45°, the two pushing wing rib are pushed out at the same time, and the water outlet holes of the two push wing rib are balanced, indicating that the stable platform is guided normally and sealed well. When the outer cylinder is rotated to 75°, the two high-side wing ribs are pushed out at the same time, and the water discharge is unbalanced. The water discharge strength near the high side is large, while the water discharge strength away from the high side is small, indicating that the stable platform is oriented normally and sealed well. When a 20mm nozzle is set, the pressure drop of the nozzle gradually increases with the increase of displacement. There is a small amount of fluid leakage at both ends of the PDC bearing, and there is also a pressure loss. The specific value can be calculated by measuring the push force. The design shape and structure of the diversion hole of the stable platform need to be further analyzed and optimized.

Based on the design presented in this paper, through a comprehensive study of the matching relationships between the performance parameters of the static push mechanical vertical drilling tool and drilling parameters (including formation rock mechanical properties), the structural performance parameters of the tool would be determined. Then four critical aspects would be completed: the eccentric stabilized platform mechanism design, push-the-bit structure design, mandrel structure design, and component manufacturing processes. Subsequently, systematic testing procedures would be conducted, including unit testing, surface integration debugging, and experimental downhole trials. Operational guidelines will then be established to implement field testing of the tool. Upon widespread application, this innovative system will achieve proactive well deviation prevention and correction. Utilizing purely mechanical components demonstrates exceptional adaptability under extreme conditions such as high temperature, high rotational speed, and vibrational impacts. The implementation is expected to deliver three key operational improvements: 1) weight on bit alleviation; 2) rate of penetration enhancement; 3) significant improvement in borehole quality.

CONCLUSIONS

This paper takes static push vertical drilling tool as the main technical background, which has solved the problems of previous vertical drilling tools, such as having too many electronic components, difficulty in dynamic precision control, and inability to withstand high temperatures and vibration shocks. Then conducts relevant research and design for its deflector disc valve, and verifies the reliability of the designed disc valve structure through horizontal bench test. The conclusions are as follows:

(1) According to the calculation results of the friction resistance of the disc valve, in order to reduce the acting area of the upper and lower fluid pressure of the disc valve, and thus reduce the effect of the friction resistance between the disc valve, the design of the convex contact structure is considered. The gap flow between the upper and the lower disc valves was simulated by finite element method, the gap between the upper and the lower disc valves should be controlled at 0.5mm, and the height of upper and lower disc valves should be controlled at 0.25mm respectively. After numerical calculation and analysis of the shut-off rule, it is considered that the designed

disc valve can meet the requirements of combining with the biased unit to realize diversion and push to control well inclination.

(2) The horizontal bench test with the optimized designed disc valve is carried out to verify the sealing and diversion performance of the designed disc valve.

(3) This paper designs the flow control disc valve of the static push type vertical drilling tool. However, it also needs to be combined with the gravity bias platform to ensure the anti-deviation effect of the tool. Furthermore, the design of the push-down device, power core shaft, PDC thrust/TC bearings and other components should be further improved to complete the design of this mechanical vertical drilling tool.

ACKNOWLEDGMENTS

The financial supports from National key plan project for research and development of China (2023YFC3009200) and (2019YFA0708300) are highly appreciated.

REFERENCES

Bai, J., Su, Y. "Theory and practice of well deviation control." Beijing: Petroleum Industry Press (1990).

Biscaro, E., D'Alessandro, J. D., Moreno, A. "New rotary steerable drilling system delivers extensive formation evaluation for high build rate wells." Paper presented at the SPE Conference, SPE 174016 (2015).

Bi, Y., Liu, G., Ma, Q., Yang, Y., Zhu, Z., Liu, J. "Static backup type rotary steering drilling tool statics characteristic analysis." Journal of Petroleum Machinery, 49(07): 1-7 (2021).

Bi, Y., Liu, G., Yang, N., Zhu, Z., Tang, H., Liu, J. "Flexible sub to static push by the influence of the rotary guide tool deflection force." Journal of Petroleum Machinery, 50(05): 9-15 (2022).

Wang, C.-C., Kuo, P.-H., Peng, T.-J., Oshima, M., Cuypers, S., Chen, Y.-T. "Voting model prediction of nonlinear behavior for double-circumferential-slot air bearing system." Chaos, Solitons & Fractals, 183: 114908 (2024).

Di, Q., Rui, Z., Zhou, X., Feng, D., Wang, C., Chen, F. "Lateral vibration characteristics of a bottom hole assembly with rotary steerable tools." Petroleum Drilling Techniques, 49(06): 8-16 (2021).

Hyland, K. B., Laing, M., O'Neill, D., Boyce, F., Keen, A., Tarn, A., Milne, R. "HPHT wells spudded utilising a rotary steerable system below a 26-in×36-in hole opener to improve tophole drilling performance." Paper presented at the SPE Conference, SPE 189639 (2018).

Jia, J., Lan, H., Jian, Z., Zhang, Y., Sun, S., Meng, W. "Bending stress distribution of type 475 static push-type rotary steerable drill assembly." Chinese Journal of Geophysics, 66(01): 95-100 (2023).

Liu, B., Chen, X., Xie, J., Zeng, L. "Research on theory and technology of automatic vertical drilling tool." Journal of Wuhan University of Science and Technology (Natural Science Edition), (01): 6-10 (2008).

Li, S., Su, Y. "Excellent performance of rotary drill assembly in Austin Chalk horizontal drilling." Foreign Petroleum Machinery, (06): 17-23 (1999).

Li, S., Wang, Y., Zhang, L., Xu, Y. "Static thrust by rotary guide control system analysis and optimization." Oil Drilling & Production Technology, 37(4): 12-15 (2015).

Li, L., Xue, Q., Liu, B., Li, X., Wang, J. "Research progress and correction behavior of mechanical automatic vertical drilling tools." Journal of Xi'an Shiyou University (Natural Science Edition), 33(01): 90-97 (2018).

Tjemsland T H H. "Evaluation of measurement-while -drilling, telemetry methods and integration of control systems. University of Stavanger, Norway (2012).

Peng, Y., Yan, W., Li, J. "Optimization design of steering force for rotary steerable drilling tools." Petroleum Drilling Techniques, (02): 10-14 (2006).

Ramalakshmi, M., Dodagoudar, R. G. "Lateral response analysis of GRS bridge abutments under passive push." Geotechnical Engineering Journal of the SEAGS & AGSSEA, 49(4) (2018).

Shi, Y., Teng, Z., Bai, J., Guan, Z., Wang, H. "Analysis on the weight-on-bit transmission efficiency of the static push-the-bit rotary steerable system." Natural Gas Industry B, 6(3): 250-256 (2019).

Shi, Y., Teng, Z., Bai, J., Guan, Z., Liu, Q., Wang, H., Fan, Z. "Improved static push-type rotary steerable drill assembly mechanical model." Journal of China University of Petroleum (Natural Science Edition), 42(05): 75-80 (2018).

Shi, Y., Sun, H., Yue, B., Guan, Z., Wang, H., Miao, Z. "Design method for anti-self-locking of static push-type rotary steerable drilling tool." Journal of China University of Petroleum (Edition of Natural Science), 41(05): 80-86 (2017).

Shi, Y., Yue, D., Zhang, D., Fu, C., Zhang, E., Chang, D., Shao, G. "Static thrust by type guide ribs into risk analysis of borehole wall." Oil Drilling & Production Technology, 43(6): 713-718 (2021).

Su, Y. "A new field in oil and gas well engineering -- well deviation control engineering." Geological Science and Technology Information, 24(S1): 1-8 (2005).

Peng, T.-J., Kuo, P.-H., Huang, W.-C., Wang, C.-C. "Nonlinear dynamic analysis and forecasting of symmetric aerostatic cavities bearing systems." International Journal of Bifurcation and Chaos, 34(04): 2430008 (2024).

Wang, H., Sun, M., Zhang, J., Guan, Z., Shi, Y., Sun,

L. "Static push by rotary steering tool build-up rate forecast analysis." Journal of Petroleum Machinery, 49(02): 15-21 (2021).

Yang, C., Wang, R., Han, L. "Dynamic safety evaluation method of BHA in push-type rotary stewing system." Journal of China University of Petroleum (Natural Science Edition), 44(02): 64-70 (2020).

Zhang, S. "New progress and development direction of modern guided drilling technology." Acta Petrolei Sinica, 24(3): 82-89 (2003).

Zhou, Q., Yao, A. "Realization of deviation correction principle and hydraulic technology of automatic directional control vertical drilling system." Mining Machinery, (11): 7-9+4 (2003).

Zhu, J., Zou, D., Zhang, Y., Hou, Y. "Design and experimental study of non-contact power transmission device in static push-type rotary steering drilling system." Advances in Petroleum Exploration and Development, 18(1): 73-82 (2019).